PHYSICAL REVIEW E

STATISTICAL PHYSICS, PLASMAS, FLUIDS, AND RELATED INTERDISCIPLINARY TOPICS

THIRD SERIES, VOLUME 53, NUMBER 4 PART B APRIL 1996

ARTICLES

Twisting transition in a fiber composed of chiral smectic-C liquid crystal polymer

R. A. Sones and R. G. Petschek
Department of Physics, Case Western Reserve University, Cleveland, Ohio 44106-7079

D. W. Cronin
Loomis Laboratory of Physics, University of Illinois, Urbana, Ilinois 61801

E. M. Terentjev
Cavendish Laboratory, Cambridge University, Cambridge CB3 0HE, United Kingdom

(Received 17 January 1995)

We consider a cylindrical fiber composed of main-chain liquid crystal polymer in the chiral smectic-C phase. Due to steric constraints on the liquid crystal polymer, the smectic layers orient perpendicular to the fiber axis, the liquid crystal director lies flat against the fiber wall, and a line disclination appears along the fiber axis. Using a Landau–de Gennes expression for the elastic free energy, we show that the fiber may undergo a transition from a cylinder to a helix. The transition is favored by large chirality, large fiber radius, and low surface tension, but is probably not experimentally accessible. However, a related transition involving only the disclination should be observable.

PACS number(s): 61.30.Cz, 61.41.+e, 64.70.Md, 83.70.Jr

I. INTRODUCTION

Liquid crystal molecules typically have rodlike shapes and exhibit various liquid crystalline phases. In the nematic phase the rodlike molecules tend to orient along a particular direction (described by the unit vector $\hat{\mathbf{n}}$, called the director), but there remains full translational symmetry. At lower temperatures smectic-A (denoted S_A) and smectic-C (denoted S_C) phases may appear, where the molecules are stacked in flat layers and show a high degree of orientational ordering, but have no positional ordering within a given layer. In the smectic-A phase the director is normal to the layers, while in the smectic-C phase it tilts slightly from the layer normal. The smectic-C geometry is depicted in Fig. 1, where θ denotes the tilt angle (typically 0° to 30°) and $\mathbf{c}$ is the component of $\hat{\mathbf{n}}$ parallel to the layers. If the molecules are noncentrosymmetric, then a chiral smectic-C phase (denoted S_C^*) may occur, where the director not only tilts but also tends to rotate about the layer normal as one moves from layer to layer, with a typical wave number (in bulk material) of $q^* \sim 10^6$ m^{-1}. The S_C^* phase is, in general, ferroelectric, with an electric polarization vector $\mathbf{p}$ orthogonal to both $\hat{\mathbf{n}}$ and $\mathbf{c}$.

A main-chain liquid crystal polymer (LCP) molecule is composed of a chain of rodlike mesogens connected head-to-tail by semiflexible spacers. The mesogens can exhibit the same liquid crystalline phases described above; in the smectic phases, the semiflexible spacers reside between neighboring layers.

In a previous paper [1] we studied the morphology of S_C^* LCP inside a capillary. There we assumed a configuration where $\hat{\mathbf{n}}$ lies flat against the capillary wall, the smectic layers orient perpendicular to the capillary axis,

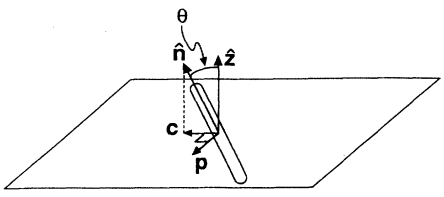

FIG. 1. Relationship between the layer normal $\hat{\mathbf{z}}$, director $\hat{\mathbf{n}}$, polarization vector $\mathbf{p}$, and $\mathbf{c}$.

and, for sufficiently small chirality, the configuration of lowest free energy has $\mathbf{p}(\mathbf{r})$ radial with a 2π disclination along the capillary axis. When chirality is increased, the disclination can shift away from the capillary axis and form a helix. The helical disclination is favored if the chirality and capillary radius are sufficiently large.

Here, as a natural extension of this previous work, we show that a fiber composed of main chain S_C^* LCP will, under certain conditions, form a helix. We assume a configuration similar to that of the capillary: the smectic layers orient perpendicular to the fiber axis, $\hat{\mathbf{n}}$ lies flat against the fiber wall, and a 2π disclination forms along the fiber axis. Surface tension at the fiber wall tends to keep it cylindrical, so if surface tension is sufficiently large the fiber and capillary problems should be identical. However, if the surface tension is sufficiently small, then the state of lowest free energy may involve deformation of the fiber away from a simple cylindrical shape. An obvious and plausible deformation to consider is one in which the fiber itself becomes helical—which is the focus of this paper.

Note that we assume the fiber material has been chosen so that the surface tension at the fiber surface is minimized when $\mathbf{p}$ is normal to the surface. This is known to be possible for low-molecular-weight S_C liquid crystals. Since the energy cost of the disclination grows slowly (logarithmically) with the radius of the fiber while the surface energy grows linearly, it is expected that, at least for large radii (as observed experimentally in a physically similar situation [2]), the surface energy will dictate the orientation of $\mathbf{p}$ at the fiber surface.

It has been shown that, due to steric constraints [3], surfaces containing the director of a main chain nematic liquid crystal are likely to have significantly lower free surface tension than other surfaces. Similar behavior is expected for main-chain S_C liquid crystals, so that *at least* one direction perpendicular to the order parameter $\mathbf{p}$ (such as $\hat{\mathbf{n}}$ or $\mathbf{c}$) is expected to lie in a low-energy surface. It is conceivable that *both* directions perpendicular to $\mathbf{p}$ should be expected to lie in a low-energy surface, which would induce $\mathbf{p}$ to be perpendicular to the surface. These considerations are consistent with our assumption that $\mathbf{p}$ is normal to the fiber surface.

In Sec. II we use a Landau–de Gennes expression for elastic free energy to determine under what conditions the equilibrium structure of the fiber is a helix. To simplify matters we assume that the fiber cross section remains circular in the helical state. In Sec. III we argue that the results of Sec. II do not change qualitatively if the fiber cross section becomes noncircular in the helical state. In Sec. IV we compare the twisting transition to previously published results and briefly discuss the feasibility of experimental observation.

II. TWISTING TRANSITION

Consider a fiber composed of S_C^* LCP, with the smectic layers stacked along the direction of the fiber (z axis). Assume that the smectic layers are ideal (flat and uniformly spaced) and that the tilt angle θ (assumed positive) is spatially invariant. Then the free energy density at any point within the fiber may be written [4]

$$\begin{aligned}\mathcal{F} = {} & \frac{K_1 c^2}{2}(\boldsymbol{\nabla}\cdot\hat{\mathbf{c}})^2 + \frac{K_2 c^2}{2}(\hat{\mathbf{c}}\cdot\boldsymbol{\nabla}\times\hat{\mathbf{c}} + q^*)^2 \\ & + \frac{K_3 c^2}{2}(\hat{\mathbf{z}}\cdot\boldsymbol{\nabla}\times\hat{\mathbf{c}})^2 \\ & - K_4 c^2(\hat{\mathbf{c}}\cdot\boldsymbol{\nabla}\times\hat{\mathbf{c}} + q^*)(\hat{\mathbf{z}}\cdot\boldsymbol{\nabla}\times\hat{\mathbf{c}}),\end{aligned} \tag{1}$$

where the K's are elastic constants with units of force, $\hat{\mathbf{c}}$ is a unit vector along $\mathbf{c}$, and $c = \sin\theta$ is the magnitude of $\mathbf{c}$. (We neglect electrostatic contributions to the free energy since these contributions are usually small and ionic impurities typically screen the polarization charge [5].) The stability of the S_C structure imposes the constraints $K_1, K_2, K_3 > 0$ and $K_2 K_3 > K_4^2$, and, in an S_C LCP, one expects $K_2 \sim K_3$ and the ratio K_1/K_2 to be of the order of the degree of polymerization [6–10]. If $\tilde{\omega}$ is the angle between $\mathbf{c}$ and $\hat{\mathbf{x}}$, then

$$\hat{\mathbf{c}} = \cos\tilde{\omega}\,\hat{\mathbf{x}} + \sin\tilde{\omega}\,\hat{\mathbf{y}}. \tag{2}$$

Define the vector $\mathbf{p} = \hat{\mathbf{z}}\times\mathbf{c}$, which is everywhere in the xy plane and makes an angle $\omega = \tilde{\omega} + \frac{\pi}{2}$ with $\hat{\mathbf{x}}$. (Using this definition, the polarization in a chiral S_C is either parallel or antiparallel to $\mathbf{p}$. In a nonchiral material, $\mathbf{p}$ is simply a more convenient field for our purposes.) Substituting (2) into (1) and expressing the result in terms of the scalar field ω gives

$$\begin{aligned}\mathcal{F} = {} & \frac{K_1 c^2}{2}(\cos\omega\,\omega_x + \sin\omega\,\omega_y)^2 + \frac{K_2 c^2}{2}(\omega_z - q^*)^2 \\ & + \frac{K_3 c^2}{2}(\sin\omega\,\omega_x - \cos\omega\,\omega_y)^2 \\ & - K_4 c^2\omega_z(\sin\omega\,\omega_x - \cos\omega\,\omega_y),\end{aligned} \tag{3}$$

where

$$\omega_x = \left(\frac{\partial\omega}{\partial x}\right)_{yz} \tag{4}$$

and so forth. Note that the $K_4 c^2 q^*$ term in (1) has been omitted from (3). This term is proportional to the divergence of $\hat{\mathbf{p}}$, so it only contributes to the free energy at the fiber surface. We assume this surface energy is substantially independent of small distortions in the field ω and lump it together with other surface energies as surface tension. Also note that, in bulk material, the free energy [the volume integral of (3)] is minimized by the uniform rotation $\omega = q^* z$.

If the fiber material is nonchiral ($q^* = 0$), the fiber assumes a cylindrical shape and the solution that minimizes the free energy is apparent from considerations of symmetry: the $\mathbf{p}$ field is radial, with $\omega = \arctan(y/x)$. This gives rise to a singularity (2π disclination) along the cylinder axis, corresponding to a filamentary core of "melted" material [11–14]. This melted core has free energy per unit length F_c and a circular cross section of radius $\rho_0 \sim 10^{-8}$ m.

When chirality is introduced the solution may change. It is plausible that a chiral material may reduce its free energy if the center of the fiber forms a helix. We parametrize the helix by its radius a and wave number q and note that the nonhelical solution corresponds to

$a = 0$. For the sake of simplicity and concreteness we assume that the melted core remains in the center of the fiber, that the melted core and fiber both maintain circular cross sections perpendicular to $\hat{\mathbf{z}}$, and that F_c, ρ_0, and the fiber radius R are independent of a and q.

The free energy per unit length in the z direction is

$$F = F_c + 2\pi R\Gamma\sqrt{1+q^2a^2} + \iint_{\mathcal{A}} \mathcal{F}(x,y,0)\,dx\,dy\,, \quad (5)$$

where Γ is the surface tension, $\mathcal{A}$ denotes the cross-sectional area of the fiber excluding the melted core region, and we evaluate $\mathcal{F}(x,y,z)$ at $z=0$ for convenience, since a uniform helical fiber must have F independent of z. The factor $2\pi R\sqrt{1+q^2a^2}$ is the surface area of the fiber per unit length in the z direction. The free energy per unit length of the nonhelical configuration is

$$F_0 = F_c + 2\pi R\Gamma + \iint_{\mathcal{A}} \mathcal{F}_0(x,y)\,dx\,dy\,, \quad (6)$$

where $\mathcal{F}_0(x,y)$ is the free energy density when $a=0$.

In principle, for given material constants and fiber radius and subject to the boundary condition that $\hat{\mathbf{n}}$ lies flat against the fiber surface, one could determine the field ω and the values of q and a, which minimize the free energy; nonzero q and a would signal a helical equilibrium state. To make the calculation tractable, we take a simpler, approximate approach: we determine exact solutions for ω at the surface of the fiber and in the vicinity of the disclination and then interpolate to estimate the form of ω elsewhere. The minimum free energy we calculate based on this approximation will be an upper bound to the true minimum.

Let $\mathbf{r}$ be an arbitrary point within the helical fiber and consider the vector $\mathbf{r}_d$ that is parallel to the xy plane and stretches from the disclination to $\mathbf{r}$. If ρ is the length of $\mathbf{r}_d$ and ϕ the angle it makes with $\hat{\mathbf{x}}$, then

$$\begin{aligned}\mathbf{r}(\rho,\phi,z) = {} & [a\cos(qz) + \rho\cos\phi]\,\hat{\mathbf{x}} \\ & + [a\sin(qz) + \rho\sin\phi]\,\hat{\mathbf{y}} + z\,\hat{\mathbf{z}}\,. \end{aligned} \quad (7)$$

Note that ρ and ϕ may be viewed as the radial and azimuthal coordinates in a coordinate system whose origin follows the disclination while its axes remain parallel to $\hat{\mathbf{x}}$, $\hat{\mathbf{y}}$, and $\hat{\mathbf{z}}$. The locus of the surface of the fiber is $\mathbf{r}(R,\phi,z)$, so the vectors

$$\begin{aligned}\mathbf{r}_\phi(R,\phi,z) &= \left(\frac{\partial}{\partial\phi}\mathbf{r}(R,\phi,z)\right)_z\,, \\ \mathbf{r}_z(R,\phi,z) &= \left(\frac{\partial}{\partial z}\mathbf{r}(R,\phi,z)\right)_\phi \end{aligned} \quad (8)$$

are both tangential to the surface of the fiber. The requirement that, at the surface the director is parallel to the surface can be written

$$\hat{\mathbf{n}}\cdot[\mathbf{r}_\phi(R,\phi,z)\times\mathbf{r}_z(R,\phi,z)] = 0\,, \quad (9)$$

where

$$\begin{aligned}\hat{\mathbf{n}} = {} & \sin\theta\,\sin[\omega(R,\phi,z)]\,\hat{\mathbf{x}} \\ & - \sin\theta\,\cos[\omega(R,\phi,z)]\,\hat{\mathbf{y}} + \cos\theta\,\hat{\mathbf{z}}\,. \end{aligned} \quad (10)$$

Equations (7)–(10) imply

$$\begin{aligned}\sin[\omega(R,\phi,z)] &= \Psi\,\sin(\phi-qz)\,\cos\phi \\ &\quad \pm \sin\phi\,\sqrt{1-[\Psi\,\sin(\phi-qz)]^2}\,, \\ \cos[\omega(R,\phi,z)] &= -\Psi\,\sin(\phi-qz)\,\sin\phi \\ &\quad \pm \cos\phi\,\sqrt{1-[\Psi\,\sin(\phi-qz)]^2}\,, \end{aligned} \quad (11)$$

where $\Psi = qa\,\cot\theta$ and both upper or both lower signs are taken. Equations (11) reduce to the correct nonhelical solution $\omega(R,\phi,z) = \pm\phi$ when $\Psi = 0$. In order for $\sin\omega$ and $\cos\omega$ to be real for all ϕ we must have $|\Psi| \le 1$ or, equivalently, $|q|a \le \tan\theta$. This condition has a simple geometric interpretation: the slope of the fiber wall (the ratio of the rise in the z direction to the run in the xy plane) cannot exceed the slope of the director; otherwise the director could not be parallel to the fiber wall.

Equations (11) are valid at the surface of the fiber ($\rho = R$). At the disclination ($\rho \to 0$) we expect $\mathbf{p}$ to be radial. We seek a general expression for $\omega(\rho,\phi,z)$, which is defined throughout the interval $0 \le \rho \le R$ and behaves properly at $\rho = R$ and as $\rho \to 0$. A plausible form for this expression can be obtained by inspection of (11): simply replace Ψ with $\Psi\rho/R$ to get

$$\begin{aligned}\sin[\omega(\rho,\phi,z)] &= \sigma\rho\,\sin(\phi-qz)\,\cos\phi \\ &\quad \pm \sin\phi\,\sqrt{1-[\sigma\rho\,\sin(\phi-qz)]^2}\,, \\ \cos[\omega(\rho,\phi,z)] &= -\sigma\rho\,\sin(\phi-qz)\,\sin\phi \\ &\quad \pm \cos\phi\,\sqrt{1-[\sigma\rho\,\sin(\phi-qz)]^2}\,, \end{aligned} \quad (12)$$

where $\sigma = \Psi/R$. For given R and θ, these equations completely determine $\omega(\rho,\phi,z)$ in terms of the helix parameters q and a. We are now in a position to use this (approximate) form of ω to calculate the free energy.

The partial derivatives of ω that appear in the free energy density (3) are calculated with respect to the xyz coordinate system, e.g., ω_z is the partial derivative of ω with respect to z, holding x and y constant. Keeping this in mind and making use of the coordinate transformations

$$\begin{aligned} x &= a\cos(qz) + \rho\cos\phi\,, \\ y &= a\sin(qz) + \rho\sin\phi\,, \end{aligned} \quad (13)$$

one finds

$$\begin{aligned}\omega_x(x,y,z) &= -\frac{\sin\phi}{\rho}\,, \\ \omega_y(x,y,z) &= \frac{\cos\phi}{\rho} \pm \frac{\sigma}{\sqrt{1-(\sigma\rho\,\sin\phi)^2}}\,, \\ \omega_z(x,y,z) &= -\frac{qa\,\cos\phi}{\rho} \mp \frac{q\sigma(a+\rho\,\cos\phi)}{\sqrt{1-(\sigma\rho\,\sin\phi)^2}}\,. \end{aligned} \quad (14)$$

Then

$$\begin{aligned}\mathcal{F}(\rho,\phi,0) = {} & \frac{K_1c^2}{2}\,I_1^2 + \frac{K_2c^2}{2}\,(I_2-q^*)^2 \\ & + \frac{K_3c^2}{2}\,I_3^2 - K_4c^2I_2I_3\,, \end{aligned} \quad (15)$$

where

$$I_1 = \cos\omega_0\,\omega_x(x,y,0) + \sin\omega_0\,\omega_y(x,y,0)$$
$$= 2\sigma\sin\phi \pm \frac{\sigma^2\rho\sin\phi\cos\phi}{\sqrt{1-(\sigma\rho\,\sin\phi)^2}},$$
$$I_2 = \omega_z(\rho,\phi,0),$$
$$I_3 = \sin\omega_0\,\omega_x(x,y,0) - \cos\omega_0\,\omega_y(x,y,0)$$
$$= -\sigma\cos\phi \pm \frac{2(\sigma\rho\,\sin\phi)^2 - 1}{\rho\sqrt{1-(\sigma\rho\,\sin\phi)^2}},$$

and $\omega_0(x,y) = \omega(x,y,0)$. The free energy density of the nonhelical configuration [let $a \to 0$ in (15)] is

$$\mathcal{F}_0(\rho,\phi) = \frac{K_2c^2}{2}(q^*)^2 + \frac{K_3c^2}{2}I_0^2, \tag{16}$$

where $I_0 = 1/\rho$.

The difference in free energy per unit length between the helical and nonhelical configurations is

$$\Delta F = F - F_0 \tag{17}$$
$$= 2\pi R\Gamma\left[\sqrt{1+(\tan\theta\,\Psi)^2} - 1\right]$$
$$+ \int_0^{2\pi} d\phi \int_{\rho_0}^{R} d\rho\,\rho\,(\mathcal{F} - \mathcal{F}_0).$$

The integrals are calculated in the Appendix. For given R and ρ_0 and for given material constants, our goal is to minimize ΔF with respect to the helix parameters q and a. We will find it convenient to do the analysis in terms of the dimensionless parameters $\Psi = qa\,\cot\theta$ and $\Phi = qR$, instead of q and a.

First, consider the case when $|\Psi| \ll 1$, corresponding to weak helicity. Expanding ΔF to lowest nonvanishing order in Ψ gives (see the Appendix)

$$\Delta F = \frac{\pi K_2c^2\Psi^2}{4}\left(\frac{\Phi^2}{2} \pm B\Phi + C\right), \tag{18}$$

where

$$B = 2\,\tan\theta - \frac{4K_4}{3K_2},$$
$$C = \frac{4K_1 - 2K_3 - 12K_4\,\tan\theta + 4R\Gamma\,\sec^2\theta}{K_2}$$
$$+2\,\tan^2\theta\,\ln(R/\rho_0) \pm 4\,\tan\theta\,\Phi^*,$$

and $\Phi^* = q^*R$. Minimizing with respect to Φ gives $\Phi = \mp B$ and

$$\Delta F = \frac{\pi K_2c^2\Psi^2}{4}\left(C - \frac{B^2}{2}\right). \tag{19}$$

For $C \geq B^2/2$ the nonhelical solution ($\Psi = 0$) is a minimum of the free energy, representing a stable or metastable state. When $C < B^2/2$ the nonhelical solution is unstable and a helix must form.

Recall that $K_1 \gg K_2 \sim K_3 \gg K_4$ [see the discussion below (1)]. To simplify the analysis, take $K_4 = 0$, neglect terms of order K_2 and K_3 compared to terms of order K_1, and assume $\tan^2\theta\,\ln(R/\rho_0) \lesssim 1$. Then only three terms of ΔF are significant: the chiral driving term (which contains q^*), the surface tension term (which contains Γ), and the K_1 term. The condition $C \geq B^2/2$ becomes

$$|q^*|R > \frac{K_1 + \Gamma R\,\sec^2\theta}{K_2\,\tan\theta}. \tag{20}$$

When this condition is fulfilled the nonhelical solution is unstable.

The analysis for $|\Psi| \ll 1$ tells us when the nonhelical solution is unstable and indicates that a twisting transition is indeed possible. But to determine the actual equilibrium configuration we must minimize ΔF for arbitrary Ψ. Keeping only the dominant q^*, Γ, and K_1 terms, we find

$$\Delta F(\Psi) \simeq \frac{K_1c^2\,J_{11}(\Psi)}{2} - K_2c^2q^*J_2(\Psi) \tag{21}$$
$$+\pi R\Gamma\,(\tan\theta\,\Psi)^2,$$

where the J's are given in the Appendix and we have taken

$$\sqrt{1+(\tan\theta\,\Psi)^2} \simeq 1 + \frac{(\tan\theta\,\Psi)^2}{2} \tag{22}$$

since, typically, $\tan^2\theta \ll 1$. Numerical exploration of $\Delta F(\Psi)$ reveals (see Fig. 2) that extrema occur only for Ψ=0,1, corresponding to either no helicity ($a = 0$) or maximum helicity ($qa = \tan\theta$). Since $\Delta F(0) = 0$, when $\Delta F(1) < 0$ the fiber will form a maximum-helicity helix. The free energy integrals can be evaluated exactly for $\Psi = 1$ and the condition $\Delta F(1) < 0$ becomes (see the Appendix)

$$|q^*|R > \frac{\pi}{4\eta}\left(\frac{K_1 + \Gamma R\,\sec^2\theta}{K_2\,\tan\theta}\right), \tag{23}$$

where $\eta \simeq 0.92$ is Catalan's constant. When this condition is fulfilled the helical solution has lower free energy than the nonhelical solution. The parameter Φ appears

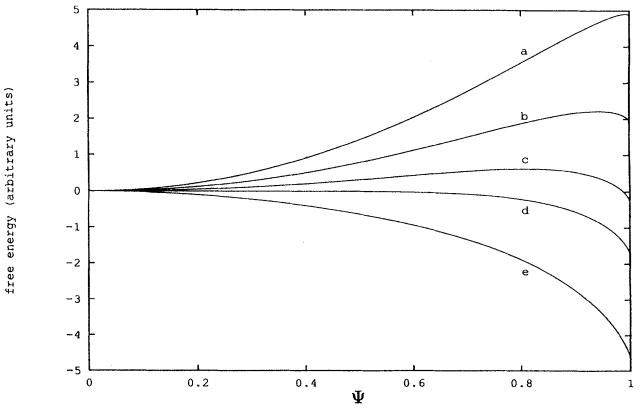

FIG. 2. Free energy (per unit length) versus Ψ for various values of chirality. The qualitative features of this plot do not depend on the values of the various parameters. Chirality increases as one moves from the top curve a to the bottom curve e. For curves a and b the equilibrium state is nonhelical ($\Psi = 0$), while for curves c–e the equilibrium state is helical ($\Psi = 1$). For chirality larger than that corresponding to curve d the nonhelical state is unstable.

only in the expression for J_{22} (see the Appendix); minimization with respect to Φ is straightforward and yields

$$|q|R = \frac{6(4-\pi)\tan\theta}{\pi} \simeq 1.64\tan\theta\,, \tag{24}$$

where q has the same sign as q^*. This determines the wave number of the helix. From $qa = \tan\theta$ we find the radius of the helix

$$\frac{a}{R} = \frac{\pi}{6(4-\pi)} \simeq 0.61\,. \tag{25}$$

Note the similarity between conditions (20) and (23). If $|q^*|$ is so large that both conditions are satisfied, then a helix is the equilibrium state and the nonhelical solution is unstable. If $|q^*|$ is reduced so that condition (23) is satisfied but (20) is not, then a helix is the equilibrium state and the nonhelical solution is metastable. If $|q^*|$ is so small that neither condition is satisfied, then the nonhelical solution represents equilibrium and a helix may or may not be metastable (we have not calculated how small $|q^*|$ must be in order for the helical solution to become unstable). Whenever a helix does form, its wave number and radius are given by (24) and (25). These are our central results.

III. NONCIRCULAR CROSS SECTION

In the preceding analysis we assumed the melted core was a helix of radius a and wave number q and that the locus of the fiber wall was $\rho(\phi) = R$, with ρ and ϕ referred to a coordinate system whose origin follows the melted core. In the limit of small a (or small $|\Psi|$) we found that ΔF goes as a^2 (or Ψ^2) and exhibits a twisting transition [see (19)]. Does this result change qualitatively if a more general chiral geometry is considered? In particular, does the chiral driving term $K_2 c^2 q^* \omega_z$ in (3) ever yield a term in ΔF that goes as a for small a? If so, this term would dominate for sufficiently small a and a helical fiber would always be favored. In this section we address this issue: we assume the melted core is still a helix but let the fiber cross section be noncircular with the locus of the fiber wall given by

$$\mathbf{r}(\phi, z) = R(\phi - qz)\,\hat{\boldsymbol{\rho}} + z\hat{\mathbf{z}}\,, \tag{26}$$

where $R(\phi)$ is an arbitrary function.

At the fiber wall and in the $z = 0$ plane, (9), (10), and (26) give

$$\begin{aligned} 0 = {} & R(\phi)\,\sin(\omega_0 - \phi) + R'(\phi)\,\cos(\omega_0 - \phi) \\ & + \cot\theta\, qR(\phi)\,R'(\phi)\,, \end{aligned} \tag{27}$$

where the prime denotes differentiation and ω_0 is the angle between $\mathbf{p}$ and the x axis. We are interested in the behavior for small a, so we assume the fiber is only slightly—and smoothly—distorted from the nonchiral configuration (i.e., we take $|\omega_0 - \phi| \ll 1$) and let

$$R(\phi) = R_0 + a\,f(\phi)\,, \tag{28}$$

where R_0 is the mean radius and f and its derivatives are of order unity (or less). Note that (28) implies $R', R'', \ldots \sim a$.

If we make the approximations $\sin(\omega_0 - \phi) \simeq \omega_0 - \phi$ and $\cos(\omega_0 - \phi) \simeq 1$, then (27) implies

$$\omega_0(R(\phi), \phi) \simeq \phi - (1 + \cot\theta\, qR)\frac{R'}{R} \tag{29}$$

at the fiber wall. At the disclination ($\rho \to 0$) we expect $\omega_0(\rho, \phi) = \phi$. A general expression for $\omega_0(\rho, \phi)$, which is defined throughout the fiber and behaves properly at both the disclination and the fiber wall, can be obtained by inserting the factor ρ/R in the second term of (29):

$$\omega_0(\rho, \phi) \simeq \phi - (1 - \cot\theta\, qR)\frac{\rho R'}{R^2}\,. \tag{30}$$

For a uniform helix

$$\omega(\rho, \phi, z) = \omega_0(\rho, \phi - qz) + qz\,, \tag{31}$$

and from this and (13) one can show that

$$\omega_z(\rho, \phi, 0) = q\left(1 - \omega_{0\phi} - a\,\sin\phi\,\omega_{0\rho} - \frac{a}{\rho}\,\cos\phi\,\omega_{0\phi}\right), \tag{32}$$

where the variables held constant during partial differentiation are x and y for ω_z, ρ for $\omega_{0\phi}$, and ϕ for $\omega_{0\rho}$. Equations (30) and (32) imply

$$\omega_z(\rho, \phi, 0) \simeq q(1 + \cot\theta\, qR)\frac{\rho R''}{R^2} - \frac{qa\,\cos\phi}{\rho} + O(a^2)\,, \tag{33}$$

where $O(a^2)$ represents terms of order a^2, i.e., terms containing aR', aR'', or $(R')^2$.

The contribution of the chiral driving term to the free energy is

$$F_{\mathrm{CD}} = -K_2 c^2 q^* \int_0^{2\pi} d\phi \int_0^{R(\phi)} d\rho\,\rho\,\omega_z(\rho, \phi, 0)\,, \tag{34}$$

where we have taken the limit $\rho_0 \to 0$. When (32) is substituted into (34), the integration over ρ is straightforward and one is left with the integration over ϕ. Terms containing R'' can be transformed into terms containing $(R')^2$ through integration by parts ["surface terms" vanish, since $R(\phi) = R(\phi + 2\pi)$], so these terms are of order a^2. One is left with

$$F_{\mathrm{CD}} \simeq K_2 c^2 q^* qa \int_0^{2\pi} d\phi\, R(\phi)\,\cos\phi + O(a^2)\,. \tag{35}$$

The integral, after using (28), is of order a, so F_{CD} is of order a^2. Thus the contribution of the chiral driving term to the free energy goes as a^2 for small a, even if the fiber profile is noncircular.

IV. DISCUSSION

As noted in the Introduction, in a previous paper [1] we studied a slightly different S_C^* LCP twisting transition,

namely, the transition of the disclination to a helix when the material is confined inside a capillary tube. With $K_4 = 0$, this "capillary" twisting transition occurs when

$$|q^*|R > \sqrt{\frac{2K_1 \ln(R/\rho_0)}{K_2}} \tag{36}$$

and the helical wave number and radius are

$$q = \frac{q^*}{\ln(R/\rho_0)}, \tag{37}$$

$$\frac{a}{R} = \sqrt{1 - \frac{2K_1 \ln(R/\rho_0)}{K_2(q^*R)^2}}. \tag{38}$$

The analogous results for the "fiber" twisting transition are given by (23)–(25). (Note that in [1] we mistakenly took K_3 and K_4 to be the large elastic constants in an S_C LCP, instead of K_1. The analysis in that paper is correct, but conclusions stemming from the assumption of large K_4 should be disregarded. Also note that we defined K_4 slightly differently in that paper than we do here: to make the notation consistent replace K_4 by K_4/c in [1].)

With $K_1 \gg K_2$, $\tan\theta \ll 1$, and $\ln(R/\rho_0) \sim 1$, a comparison of (23) and (36) reveals that the capillary twisting transition (i.e., helical disclination inside nonhelical fiber) occurs for smaller q^* than does the fiber twisting transition. Furthermore, no matter what the relationship between K_1 and K_2, if we use the plausible values $K_2 \sim 10^{-11}$ N [15], $\Gamma \sim 10^{-2}$ Nm^{-1} [16,17], and $\tan\theta \sim 0.1$, then (23) implies $q^* \gtrsim 10^{10}$ m^{-1} for the fiber twisting transition to occur—an unreasonably large value for q^*.

We conclude that the pure fiber twisting transition is unlikely to be observable. However, the capillary transition should be observable. Indeed, (36) implies that, for any nonzero value of q^*, the transition must occur for sufficiently large R. This can be understood physically, since, as R grows large, the interior of the fiber approaches the bulk state, which is chiral, while surface effects become less and less important. Thus there must be a twisting transition for sufficiently large R. In a S_C LCP the ratio K_1/K_2 is expected to be proportional to the polymerization index, so the value of $|q^*|R$ at the twisting transition should go as the square root of the polymerization index.

Once the capillary transition occurs and the disclination is helical, helicity may be induced in the overall fiber shape. An improved theory of the helical transitions of a S_C^* LCP fiber would have to take such disclination-fiber interactions into account.

ACKNOWLEDGMENT

This work was supported by the NSF under Grant No. DMR-91-22227.

APPENDIX: FREE ENERGY INTEGRALS

From (15)–(17) the difference in free energy per unit length between the helical and nonhelical configurations is

$$\begin{aligned}\Delta F = {} & \frac{K_1c^2}{2} J_{11} + \frac{K_2c^2}{2} J_{22} - K_2c^2q^*J_2 \\ & + \frac{K_3c^2}{2}(J_{33} - J_{00}) - K_4c^2J_{23} \\ & + 2\pi R\Gamma[\sqrt{1 + (\tan\theta\,\Psi)^2} - 1],\end{aligned} \tag{A1}$$

where

$$\begin{aligned}J_{00} &= \int d\phi \int d\rho\, \rho I_0^2 \\ &= 2\pi \ln(R/\rho_0), \\ J_{11} &= \int d\phi \int d\rho\, \rho I_1^2 \\ &= \frac{3\pi\Psi^2}{2} + 2\pi\left[1 - \sqrt{1-\Psi^2} \right. \\ &\quad \left. + \ln\left(1 + \sqrt{1-\Psi^2}\right) - \ln 2\right], \\ J_2 &= \int d\phi \int d\rho\, \rho I_2 \\ &= \mp 2 \tan\theta\, R\Psi^2 \int_0^1 du\, K(\Psi^2 u), \\ J_{22} &= \int d\phi \int d\rho\, \rho I_2^2 \\ &= \pi \tan^2\theta \ln(R/\rho_0)\,\Psi^2 + 2\pi \tan^2\theta\,\Psi^2(1 - \sqrt{1-\Psi^2}) \\ &\quad + \pi\Phi^2\left(\frac{3\Psi^2 + 2(1-\Psi^2)^{3/2} - 2}{3\Psi^2}\right) \\ &\quad \pm 8 \tan\theta\,\Phi \int_0^{\pi/2} du\, \cot^2 u\,[1 - \sqrt{1 - (\Psi \sin u)^2}], \\ J_{23} &= \int d\phi \int d\rho\, \rho I_2 I_3 \\ &= 5\pi \tan\theta\,\Psi^2 - 2\pi \tan\theta\,\Psi \sin^{-1}\Psi \\ &\quad \pm \pi\Phi\Psi^2 \int_0^1 du\, u^2 F\left(\frac{1}{2}, \frac{1}{2}; 2; \Psi^2u^2\right), \\ J_{33} &= \int d\phi \int d\rho\, \rho I_3^2 \\ &= 2\pi \ln(R/\rho_0) - \frac{3\pi\Psi^2}{2} \\ &\quad - 2\int_0^{\pi/2} du \ln\left[1 - (\Psi^2 \sin^2 u)^2\right],\end{aligned} \tag{A2}$$

$\Psi = qa\cot\theta$, $\Phi = qR$, ϕ integration is over the interval 0 to 2π, ρ integration is over the interval 0 to R (or ρ_0 to R, when appropriate), K is the complete elliptic integral of the first kind [18], and F is the hypergeometric function [18]. When $|\Psi| \ll 1$ the J integrals can be approximated by keeping terms only up to order Ψ^2:

$$
\begin{aligned}
J_{00} &= 2\pi \ln(R/\rho_0)\,, \\
J_{11} &\simeq 2\pi\Psi^2\,, \\
J_2 &\simeq \mp\pi \tan\theta\, R\Psi^2\,, \\
J_{22} &\simeq \pi\left(\tan^2\theta \ln(R/\rho_0) \pm \tan\theta\,\Phi + \frac{\Phi^2}{4}\right)\Psi^2\,, \\
J_{23} &\simeq 3\pi\left(\tan\theta \pm \frac{\Phi}{9}\right)\Psi^2\,, \\
J_{33} &\simeq 2\pi \ln(R/\rho_0) - \pi\Psi^2\,.
\end{aligned}
\tag{A3}
$$

When $|\Psi| = 1$ the J integrals become

$$
\begin{aligned}
J_{00} &= 2\pi \ln(R/\rho_0)\,, \\
J_{11} &= 2\pi\left(\frac{7}{4} - \ln 2\right)\,,
\end{aligned}
\tag{A4}
$$

$$
\begin{aligned}
J_2 &= \mp 4\eta \tan\theta\, R\,, \\
J_{22} &= \pi \tan^2\theta \ln(R/\rho_0) + 2\pi \tan^2\theta \\
&\quad \pm 4(4-\pi)\tan\theta\,\Phi + \frac{\pi\Phi^2}{3}\,, \\
J_{23} &\simeq \pi(5-\pi)\tan\theta \pm 0.372\,\pi\Phi\,, \\
J_{33} &= 2\pi \ln(R/\rho_0) - \frac{3\pi}{2} + 2\pi \ln 2\,,
\end{aligned}
$$

where

$$
\eta = \frac{1}{2}\int_0^1 du\, K(u) \simeq 0.92 \tag{A5}
$$

is Catalan's constant [19].

[1] D. W. Cronin, E. M. Terentjev, R. A. Sones, and R. G. Petschek, Mol. Cryst. Liq. Cryst. **238**, 167 (1994).

[2] C. D. Munzy and N. A. Clark, Phys. Rev. Lett. **68**, 804 (1992).

[3] E. M. Terentjev, J. Phys. (France) II **5**, 159 (1995).

[4] M. J. Stephen and J. P. Straley, Rev. Mod. Phys. **46**, 686 (1974), where $K_1 = \alpha_{11}$, $K_2 = \alpha_{22}$, $K_3 = \alpha_{33}$, and $K_4 = \alpha_{23}$.

[5] M.-H. Lu, C. Rosenblatt, and R. G. Petschek, Phys. Rev. E **47**, 1139 (1993).

[6] R. B. Meyer, in *Polymer Liquid Crystals*, edited by A. Ciferri, W. Krigbaum, and R. B. Meyer (Academic, New York, 1982).

[7] A. Y. Grosberg and A. V. Zhestkov, Polym. Sci. U.S.S.R. **28**, 97 (1986).

[8] T. Odijk, Liq. Cryst. **1**, 553 (1986).

[9] R. G. Petschek and E. M. Terentjev, Phys. Rev. A **45**, 930 (1992).

[10] R. G. Petschek and E. M. Terentjev (unpublished).

[11] J. Fousek and M. Glogarove, Ferroelectrics **53**, 71 (1984).

[12] E. B. Loginov and E. M. Terentjev, Kristallografiya **30**, 10 (1985) [Sov. Phys. Crystallogr. **30**, 4 (1985)].

[13] N. Schopohl and T. Sluckin, Phys. Rev. Lett. **59**, 2582 (1987).

[14] S. Kralj and T. Sluckin, Phys. Rev. E **48**, R3244 (1993).

[15] P. G. de Gennes and J. Proust, *The Physics of Liquid Crystals*, 2nd ed. (Clarendon, Oxford, 1993).

[16] C. I. Poser and I. C. Sanchez, Macromolecules **14**, 361 (1981).

[17] A. K. George and K. P. Mohandas, J. Phys. Condens. Matter **4**, 7691 (1992).

[18] *Handbook of Mathematical Functions*, Natl. Bur. Stand. Appl. Math. Ser. No. 55, edited by M. Abramowitz and I. A. Stegun (U.S. GPO, Washington, DC, 1970).

[19] I. S. Gradsteyn and I. M. Ryzhik, *Table of Integrals, Series and Products* (Academic San Diego, 1980).